Supporting Information

Artyukhov et al. 10.1073/pnas.1207519109

SI Text

Details of Density Function Theory (DFT) Calculations. The DFT calculations were performed with the Vienna Ab initio Simulation Package (VASP) (1, 2) using ultrasoft pseudopotentials (3, 4) for electron-ion interactions and the Ceperley–Alder (5) local density approximation for the exchange-correlation functional.

To calculate the edge energy of graphene on metal, a graphene ribbon was put on a two-layer metal slab with bottom layer fixed. Around 15 Å vacuum space was kept in the direction perpendicular to slab surface, and the distance between periodic images of the ribbon was around 10 Å to avoid interactions between the replicas. The structures were optimized using the conjugate gradient algorithm until the forces on every atom were <0.01 eV/Å. The unit cell was orthogonal in all calculations. The width of zigzag (Z) ribbon was $5\sqrt{3}a$, and the width of armchair (A) ribbon was $5a$. The reciprocal space was sampled using 5- and 9-point Monkhorst–Pack k-point grids (6) along the edge for A and Z edges, respectively. Increasing the ribbon width changed the edge energy by less than 10 meV/Å.

To calculate the energy of carbon addition, a short graphene ribbon was put on double-layer metal slab with bottom layer fixed. The nongrowing side of the ribbon was docked to a metal step (an incomplete 3rd layer, see Fig. S1). The Brillouin zone was sampled at the Γ point only. The unit cell for calculation is shown in Fig. S2. The configurations featured in Fig. 3 of the paper are listed in Figs. S3–S5.

Growth Velocity Anisotropy. ***Initial assumptions.*** Depending on edge direction χ, site types—A, Z, and K (kink)—are present in different concentrations: $s_A(\chi)$, $s_Z(\chi)$, and $s_K(\chi)$, per graphene unit cell length a_0. Each A or kink site can accept two atoms. The first is attached at a free energy cost (E_A and E_K, respectively). The second one is assumed to attach instantaneously after the first because its attachment reduces free energy. Z sites behave differently: Adding atoms to a Z edge creates two kinks having opposite directions (removing two Z sites). Such kinks will be termed extrinsic, so as to distinguish them from the intrinsic kinks [concentration, $s_K^0(\chi)$] prescribed by the edge orientation. Nucleation of two kinks has a free energy barrier, E_Z, and takes a certain critical number of atoms, N^*, and we may assume $N^* = 1$ for simplicity. (The exact value of N^* does not matter greatly because, as shown below, the main contribution to growth velocity of Z edges comes from extrinsic kinks.)

The linear growth velocity of a straight edge can be expressed as follows: $v = A\frac{dn}{dt}$, where $\frac{dn}{dt}$ is the rate of atom attachment to the edge per lattice constant a, and A is the specific area of one atom, $A = \frac{1}{2}\frac{\sqrt{3}}{2}a^2$. The total rate includes contributions from individual sites, and has the form of $dn/dt = \sum s_i f_i p_i N_i$, where the factors are site concentration per unit length, attempt frequency, acceptance probability, and the number of atoms per successful addition to a site of type i (A/Z/K).

Following the same logic as in constructing Fig. 2, the acceptance probabilities are easily obtained as $\frac{p_i}{1-p_i} = e^{-\frac{E_i-\Delta\mu}{kT}}$, producing a well-known result:

$$p_i = \frac{1}{1+e^{\frac{E_i-\Delta\mu}{kT}}} \equiv p\left(\frac{E_i-\Delta\mu}{kT}\right).$$

As for the attempt frequencies f_i, these are complicated objects factoring both the diffusion of carbon atoms on the substrate, as well as the effective cross-section of attachment site. In the simplest approximation, we may assume infinitely fast (compared to growth) diffusion, and treat each vacant site at the edge as a very narrow target that does not overlap with neighboring sites and compete with them for atoms. Then, $f_A = f_Z = f_K = F\sigma = \text{const}$, where F is the total flux of source carbon atoms, and σ is the effective cross-section of a site ($\sigma \ll 1/s_i$). We may use $(F\sigma)^{-1}$ for time units, so that each active site is visited on average once per unit time.

In principle, we should also include the Arrhenius activation energies in the f_is. Omitting them is justified if their differences are small compared to respective E_i differences. However, even if they aren't, the Brønsted–Evans–Polanyi–Semenov rule leads us to expect them to approximately correlate with E_is, in which case the effect of ignoring activation is effectively equivalent to scaling the value of kT by some factor of less than 1. Because in our case the growth velocity anisotropy increases vigorously with decreasing temperature (see Figs. 4 and S6), such scaling will not invalidate our main result about kinetically limited Z-edged hexagonal shapes.

Concentration of kinks on pristine Z edge. For clarity, in this section we assume that Δμ is small (compared to $E_Z - E_K$), and we may replace $p(\frac{E_i}{kT}) \approx e^{-E_i/kT}$.

At a pristine Z edge. There are no intrinsic kinks, and Z site concentration is $s_Z(0) = 1$. What is the equilibrium stationary concentration of (extrinsic) kinks, s_K? The probability to create, at the expense of two Z sites, a nucleus of a new atomic row is $e^{-E_Z/kT}$. Each of the two resulting kinks starts to propagate (irreversibly) along the edge with a velocity of $v_K = e^{-E_K/kT}$ (lattice constants per unit time).

Let $d = 2/s_K(0)$ be the average distance between two such nuclei (factor 2 is there because each nucleus makes two kinks). Then, the average inverse time it takes two kinks from neighboring nuclei to meet and annihilate is $\tau^{-1} = 2v_K/d = v_K s_K(0)$. Each annihilation removes two kinks, but we only need count one kink from every pair to avoid double counting, so the intensity of kink removal is $2\tau^{-1}\frac{s_K(0)}{2} = v_K \times [s_K(0)]^2$. Then, the equation for equilibrium concentration of kinks on Z edge is

$$\frac{ds_K(0)}{dt} = 0 = 2[s_Z(0) - s_K(0)]e^{\frac{-E_Z}{kT}} - [s_K(0)]^2 e^{\frac{-E_K}{kT}},$$

$$s_K(0) = e^{\frac{E_K-E_Z}{kT}}\left(\sqrt{1+2e^{\frac{E_Z-E_K}{kT}}} - 1\right).$$

Kink concentration at arbitrary orientation. For an arbitrary edge direction χ, the difference from a previous case is in the presence of a background of intrinsic kinks, all propagating in one direction. These [concentration, $s_K^0(\chi)$] can additionally annihilate with the counter-propagating extrinsic kinks. We can divide extrinsic kinks in two classes: those propagating along with the intrinsic kinks ($x+$) and the counterpropagating kinks ($x-$): $s_K^{x+} = s_K^{x-} = \frac{1}{2}s_K^x = \frac{1}{2}(s_K - s_K^0)$. The intensity of annihilation then is $2 \times 2v_K \times s_K^{x-}(s_K^{x+} + s_K^0) = 2 \times 2v_K \times \frac{1}{2}(s_K - s_K^0) \times \frac{1}{2}(s_K + s_K^0)$. The seemingly additional (comparing to the previous equation) factor of 2 is there because now we are explicitly making a distinction between positive and negative kinks, thereby avoiding double counting from the start. The resulting equation then reads, as follows:

$$\frac{ds_K(\chi)}{dt} = 0 = 2[s_Z(\chi) - s_K(\chi)]e^{\frac{-E_Z}{kT}} - [s_K(\chi) - s_K^0(\chi)] \times [s_K(\chi) + s_K^0(\chi)]e^{\frac{-E_K}{kT}}.$$

Solving for $s_K(\chi)$ and combining the result with the geometrical analysis of site concentrations (7), we can now write down the final joint expression for orientation-dependent edge growth velocity:

$$v(\chi) \propto 2s_A(\chi)p\left(\frac{E_A - \Delta\mu}{kT}\right) + 2s_K(\chi)p\left(\frac{E_K - \Delta\mu}{kT}\right) + (s_Z(\chi) - [s_K(\chi) - s_K^0(\chi)])p\left(\frac{E_Z - \Delta\mu}{kT}\right),$$

$$p\left(\frac{E_i - \Delta\mu}{kT}\right) = \frac{1}{1 + e^{\frac{E_i - \Delta\mu}{kT}}},$$

$$s_A(\chi) = \begin{cases} 0 & \chi < \beta \\ \frac{5}{\sqrt{3}}\sin\chi - \cos\chi & \chi \geq \beta \end{cases},$$

$$s_Z(\chi) = \cos\chi - \sqrt{3}\sin\chi,$$

$$s_K(\chi) = e^{\frac{E_K - E_Z}{kT}}\left[\left(1 + 2s_Z(\chi)e^{\frac{E_Z - E_K}{kT}} + (s_k^0(\chi))^2 e^{\frac{2(E_Z - E_K)}{kT}}\right)^{\frac{1}{2}} - 1\right],$$

$$s_K^0(\chi) = \begin{cases} \frac{2}{\sqrt{3}}\sin\chi & \chi < \beta \\ 2\sin\left(\frac{\pi}{6} - \chi\right) & \chi \geq \beta \end{cases}, \qquad \beta = \arctan\frac{\sqrt{3}}{5}.$$

The pristine-edge solution is correctly recovered if we substitute $s_Z^0(0) = 1$, $s_K^0(0) = 0$. At intermediate chiral angles, $s_K(\chi) \approx s_K^0(\chi)$, i.e., intrinsic kinks dominate the growth velocity. At small values of μ, the Fermi function $p_i \approx \exp(-\frac{E_i}{kT})$, as shown in the main text.

Fig. S6 provides a better feel of how the character of $v(\chi)$ changes with increasing nonequilibrium (Δμ). The top row shows polar plots at an artificially elevated temperature of 0.3 eV. Bottom plots use a more realistic value of 0.1 eV and a logarithmic scale, to accommodate for the strong anisotropy of $v(\chi)$. It can be seen that as the chemical potential becomes sufficient to overcome kink growth barrier, p_K starts to saturate, and the gap between K and A growth velocity begins to shrink. At $\Delta\mu > E_A$, A edges cease to be a local minimum of $v(\chi)$ and become a global maximum. At even greater Δμ values, $v(\chi)$ will become more and more isotropic. (In this regime, some of our assumptions may break down, however it is not of great interest, as such strongly nonequilibrium conditions are expected to produce many defects and to be prone to formation of dendritic shapes.)

Movie S1 shows an animation illustrating the changes in the nanoreactor diagram and the corresponding kinetic Wulff construction as μ is varied.

1. Kresse G, Furthmüller J (1996) Efficient iterative schemes for ab initio total-energy calculations using a plane-wave basis set. *Phys Rev B* 54:11169–11186.
2. Kresse G, Hafner J (1993) Ab initio molecular dynamics for liquid metals. *Phys Rev B* 47:558–561.
3. Vanderbilt D (1990) Soft self-consistent pseudopotentials in a generalized eigenvalue formalism. *Phys Rev B* 41:7892–7895.
4. Kresse G, Hafner J (1994) Norm-conserving and ultrasoft pseudopotentials for first-row and transition elements. *J Phys Condens Matter* 6:8245–8257.
5. Ceperley DM, Alder BJ (1980) Ground state of the electron gas by a stochastic method. *Phys Rev Lett* 45:566–569.
6. Monkhorst HJ, Pack JD (1976) Special points for Brillouin-zone integrations. *Phys Rev B* 13:5188–5192.
7. Rao R, Liptak D, Cherukuri T, Yakobson BI, Maruyama B (2012) In situ evidence for chirality-dependent growth rates of individual carbon nanotubes. *Nat Mater* 11:213–216.

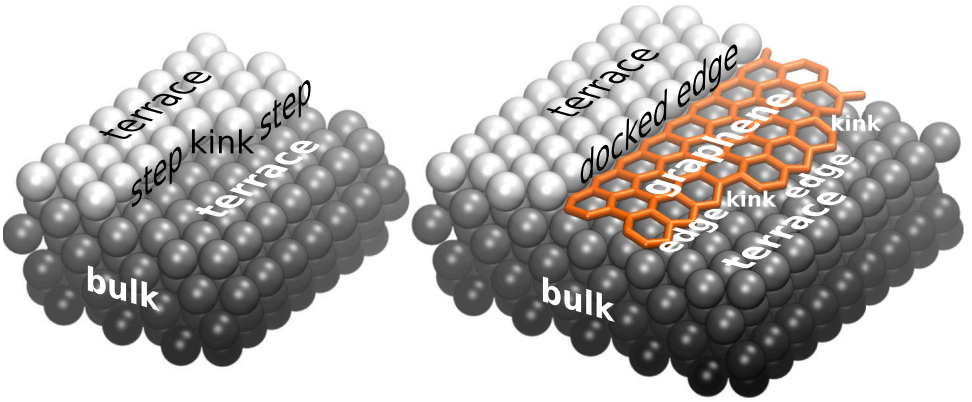

Fig. S1. Analogy between graphene edge growth and step-flow lateral growth of crystals in the canonical Burton—Cabrera—Frank representation.

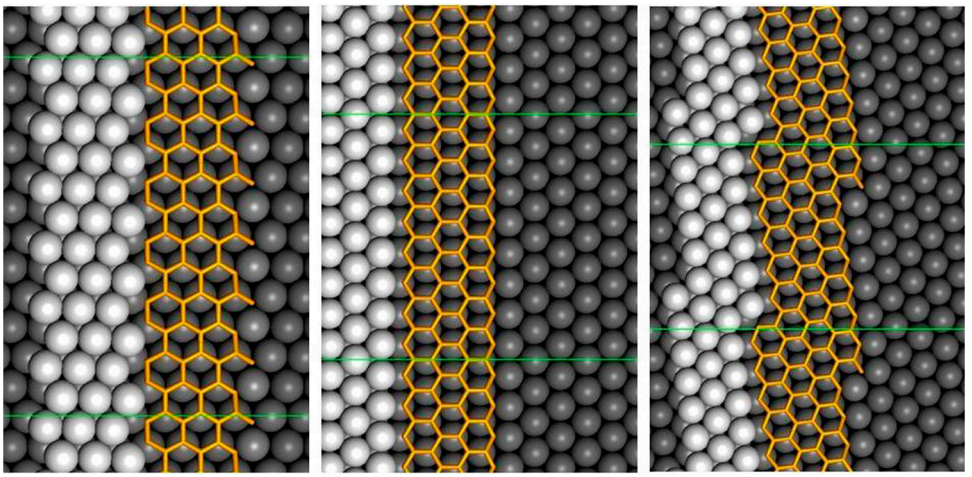

Fig. S2. Supercells used for modeling. (*Left* to *Right*) A edge, Z edge, and kink growth. Metal atoms are shown as balls with color representing depth. Orange sticks represent graphene. Green lines indicate the periodic box.

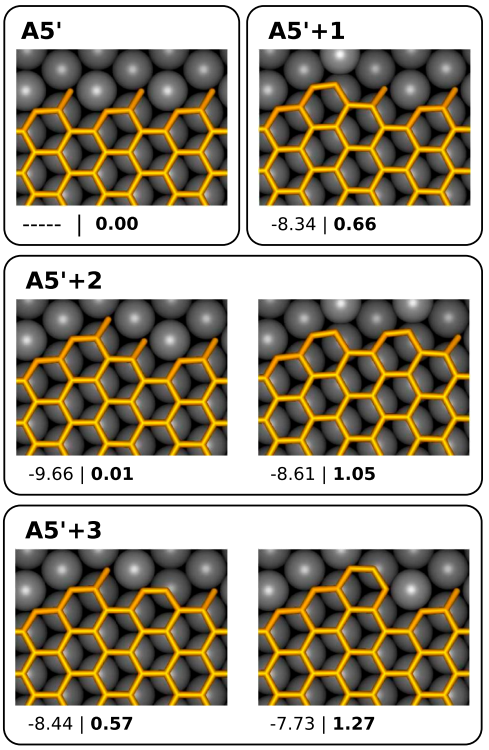

Fig. S3. Possible atomistic structures during A edge growth, with their respective values (electronvolt) of last atom's binding energy ϵ (where applicable) and formation free energy ΔG (shown in boldface).

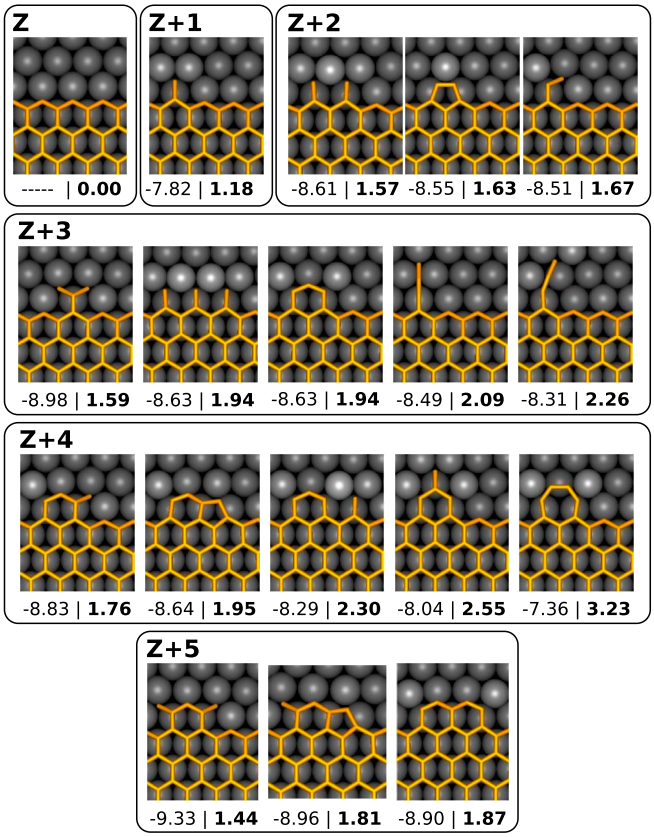

Fig. S4. Possible atomistic structures during Z edge growth, with their respective values (electronvolt) of last atom's binding energy ϵ (where applicable) and formation free energy ΔG (shown in boldface).

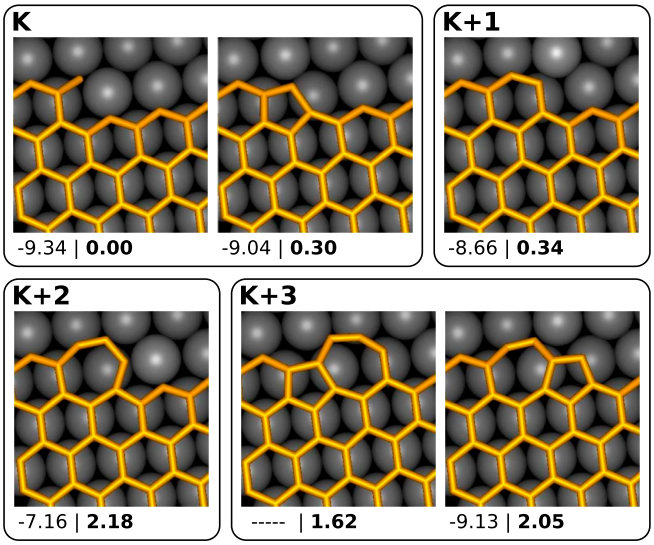

Fig. S5. Possible atomistic structures during kink growth, with their respective values (electronvolt) of last atom's binding energy ϵ (where applicable) and formation free energy ΔG (shown in boldface). (*Top*) Normal kink propagation is a cycle comprised of just two stages. (*Bottom*) formation of a (5–7) defect during kink propagation.

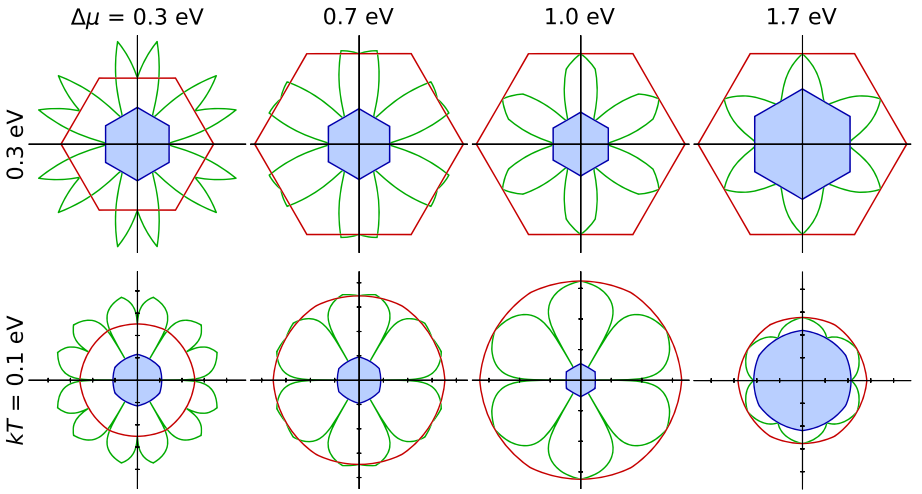

Fig. S6. Kinetic Wulff construction for graphene growth on Ni as a function of chemical potential. Each axis tick in the bottom plots corresponds to a factor-of-10 difference.

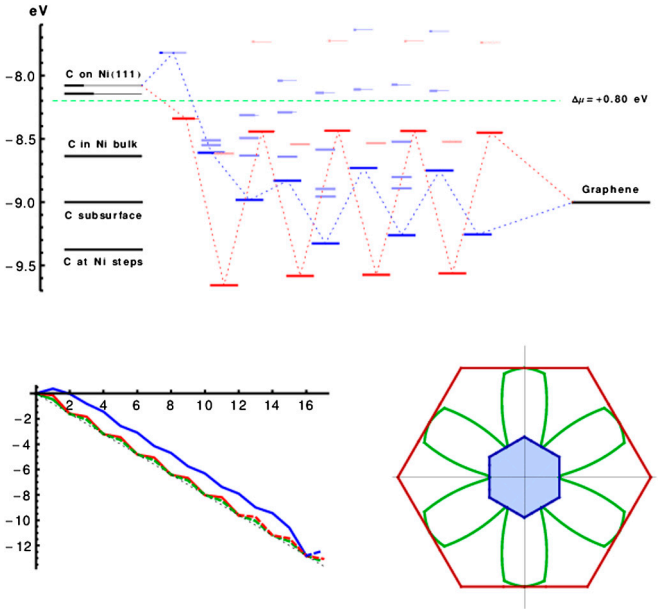

Movie S1. Animation illustrating the changes in the nanoreactor diagram and the corresponding kinetic Wulff construction as the chemical potential is varied.

Movie S1(GIF)